Non Linear Model Predictive Control (NMPC) for a Linear Take-off Procedure of an Airborne Wind Energy (AWE) System

Mohammed Saeed*, Youssef Mahran*, Zeyad Gamal*,
Royia Soliman**, Florian Holzapfel**, and Ayman El-Badawy*
*German University in Cairo (GUC), Egypt,
**Institute of Flight System Dynamics, Technische Universität München (TUM), Germany
Emails: mohammed.saeed@student.guc.edu.eg, youssef.mahran@student.guc.edu.eg, zeyad.abdrabo@student.guc.edu.eg,
royia.soliman@tum.de, florian.holzapfel@tum.de, ayman.elbadawy@guc.edu.eg

***Abstract*—A Non Linear Model Predictive Controller (NMPC) for the realization of an autonomous take-off procedure of a rigid wing Airborne Wind Energy (AWE) system is proposed. The addressed take-off approach employs a linear motion system to accelerate the aircraft to take-off speed, a winch which is connected to the aircraft with a tether, and finally on-board propellers to drive the aircraft to operational altitude. A comparison between the performance of the NMPC with the Linear Quadratic Regulator (LQR) is made to determine whether it is necessary to use advanced non-linear controllers in the considered take-off procedure. Simulations results demonstrate that the NMPC outperforms the LQR in terms of pitch angle and velocity tracking as well as time to reach a desired minimum altitude. Additionally, a comparative power analysis was conducted and results indicate that the NMPC controller is more energy efficient since it is able to drive the aircraft to a larger altitude with smaller power losses.**

I. Introduction

For the past century, the idea of generating electricity from wind energy has been gradually on the rise and today, around 5% of the world's energy is provided by wind power [1]. During the past two decades, the field of AWE has developed immensely where the use of tethered aircraft has been used to generate electricity from wind energy. This idea was first examined by the scientist Miles Loyd who investigated the ideal power production capabilities of a cross-wind kite system [2]. There are several benefits to the use of AWE systems rather than conventional Wind Turbines (WTs) to harness wind energy. Tethered aircraft are able to access high-altitude winds which have larger speeds and are more stable thus, allowing for a low levelised cost of energy that is significantly less dependent on geographic location . Previous research has shown that an AWE system with variable height of up to 500 meters has double the wind power density as a conventional WT [3]. However, the use of AWE systems poses its own set of challenges which are mainly associated with the control of the system. Generally, these systems are highly nonlinear and operate in very uncertain environments making the development of suitable and robust controllers a difficult task [4].

A typical rigid wing AWE system goes through a sequence of three states to reach the power-generating crosswind flight states. First, the system undergoes a take-off procedure which consists of a launch phase and a climb phase. The launch phase entails accelerating the aircraft to a predefined take-off speed while the climb phase consists of driving the aircraft to a minimum desired altitude. A transition state is then needed to drive the system to a velocity and position which is acceptable to begin the power generating crosswind flight. Finally, the rigid wing would start flying high-lift crosswind trajectories where the variation of tether force and length creates a net positive power cycle. This paper specifically focuses on the take-off procedure of a rigid wing AWE system. The take-off and landing of AWEs is one of the most important topics of future research in the field [5]. This is due to the scarcity of literature present discussing the control of these flight phases and their paramount role in achieving fully autonomous large-scale implementations of AWE systems.

There are four main take-off approaches for rigid-wing AWE systems [6]. These include vertical take-off with rotors, rotational take-off, linear take-off with on-board propellers, and the winch launch take-off approach. In the aforementioned study, it was found that the linear take-off with on-board propellers was the most suitable from a techno-economical point of view since it requires reasonable land area for take-off and involves relatively low on-board power demands compared to the total system power, resulting in a small cost fraction for the take-off equipment. Hence, this paper focuses specifically on the linear take-off procedure with on-board propellers.

A control approach for an autonomous linear take-off procedure is proposed [7]. The control design in this system is critical, as it must synchronize the winch reeling with the aircraft's motion while stabilizing the aircraft during its straight-line climb phase. This process involves a combination of PID controllers for the ground system and model-based approaches for the aircraft control. Simulation and experimental results demonstrate the success of this method in compact spaces, making it relevant for AWE systems in limited areas. However, this study didn't utilize non-linear control methods and focused primarily on PID control. The author recommended

the use of advanced non-linear controllers which take into account couplings, non-linearities, and tether force disturbances to enhance the linear take-off approach with on-board propellers.

Another study proposed a decoupled control approach for both the ground station and aircraft by approximating the tether with an elastic model whose stiffness depends on the tether length, ensuring precise coordination during the take-off phase [8]. The nonlinear dynamics of the aircraft are linearized around a trim point while neglecting the tether force and hence, a Linear Quadratic Regulator (LQR) control designed. This linearized decoupled strategy ensures minimal tether tension during take-off, which is crucial for a smooth and controlled ascent. However, this approach didn't utilize non-linear control techniques and focused primarily on linearizing and decoupling the AWE system.

Since NMPC has not been applied to the linear take-off procedure with on-board propellers, a paper which actually utilized this control strategy but for a rotational take-off approach will be introduced. A NMPC control and Moving Horizon Estimation (MHE) was designed to control the rotational take-off of tethered airplanes in AWE systems [9]. NMPC optimizes the aircraft's trajectory during take-off while directly handling nonlinearities and constraints, and the MHE provides real-time estimation of the system states ensuring accurate and robust control in the presence of uncertainties. Simulation results demonstrate the system's ability to handle dynamic wind conditions, making it effective for stable and controlled take-off. However, this approach has been applied to rotational take-off methods only and does not address the linear take-off procedure.

This paper aims to implement an advanced non-linear controller in the form of a NMPC to control the aircraft during the linear take-off procedure of a rigid wing AWE system. The take-off procedure consists two states, which are the launch state where the aircraft is accelerated to take-off speed and the climb state, where the aircraft is driven to reach a desired altitude. Furthermore, the performance of the NMPC is compared to a LQR controller to assess if the latter is sufficient to control the aircraft in the take-off phase, especially when tether forces appear which may drive the system away from its trim point, or will a NMPC controller be needed to adequately handle the input constraints, tether forces, and inherent non-linearities of the system. Finally, a power analysis is conducted to compare the LQR and NMPC controllers in terms of the total power required for the linear take-off procedure.

II. Methodology

A. AWE System Description

The system presented in this paper includes a ground station which consists of a winch motor, a slide motor, and a tether connecting the aircraft to the winch where the tether force causes couplings between the ground station and the aircraft. The winch motor is utilized mainly in the power production phase where it achieves high tether forces in the traction phase and maintains low tether forces in the retraction phase creating a net positive energy cycle. The slide motor on the other hand is connected to a linear motion system with the aim of accelerating the aircraft to take-off speed where it the employs its propellers to gain altitude. The system considered in this paper is that of [8] however, in this paper, a NMPC controller is employed to control the aircraft in the climb state as opposed to a LQR controller in the aforementioned paper. However, the ground station which consists of the winch and slide motors is controlled using linear PID controllers. Fig. 1 shows the platform from which the aircraft takes-off from while exhibiting the system in its different operational states.

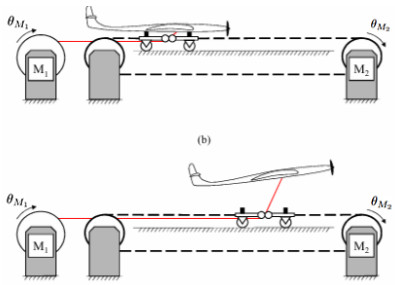

Fig. 1. Sketch showing the winch motor M_1 and the slide motor M_2 as well as the launch state where the aircraft and the slide are still attached (a), and the climb state where the aircraft is detached from the slide (b) [8]

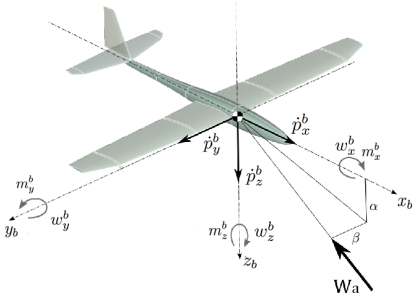

Fig. 2. Sketch showing the aircraft body-fixed linear and angular velocities, the body-fixed moments applied, and the angle-of-attack and side-slip angles [10]

B. AWE System Modelling

The dynamical system consists of two states where the first state describes the system dynamics during the launch state and the second state describes the system dynamics during the climb state. During the launch state, the aircraft and the slide are attached and thus, they can be considered as one rigid body. Thus, the states of the system consist of the angular position and velocity of the winch motor $(\theta_{M_1}, \dot{\theta}_{M_1})$ respectively and the angular position and velocity of the slide motor $(\theta_{M_2}, \dot{\theta}_{M_2})$ respectively as shown in Eq. 1.

$$\mathbf{x}_{launch} = [\theta_{M_1}, \dot{\theta}_{M_1}, \theta_{M_2}, \dot{\theta}_{M_2}] \tag{1}$$

The control inputs are the torque of the winch u_{M_1} and the torque of the slide u_{M_2} as shown in Eq. 2.

$$\mathbf{u}_{launch} = [u_{M_1}, u_{M_2}] \tag{2}$$

The dynamical equations describing the system during the launch phase are as follows:

$$\ddot{\theta}_{M_1} = \frac{1}{J_{M_1}} \left(r_{M_1} \|\mathbf{f}_t^{\mathbf{b}}\|_2 - \beta_{M_1} \dot{\theta}_{M_1} + u_{M_1} \right) \tag{3}$$

$$\ddot{\theta}_{M_2} = \frac{1}{J_{M_2} + (m_s + m_r) r_{M_2}^2} \big(- r_{M_2} \|\mathbf{f}_t^{\mathbf{b}}\|_2 - \beta_r r_{M_2}^2 \dot{\theta}_{M_2} - \beta_{M_2} \dot{\theta}_{M_2} + u_{M_2} \big) \tag{4}$$

Where r_{M_1} is the radius of the winch drum, r_{M_2} is the radius of the pulley linking the slide motor to the belt, J_{M_1} is the mass moment of inertia of the winch motor and its drum, J_{M_2} is that of the slide motor and its pulley, β_{M_1} and β_{M_2} are the viscous friction coefficients of the winch and slide motors respectively, and β_s is the viscous friction coefficient of the belt system attached to the slide motor. Additionally, m_s is the mass of the slide, m is the mass of the aircraft, and $\|\mathbf{f}_t^{\mathbf{b}}\|_2$ denotes the magnitude of the tether force acting on the aircraft.

The switch between the two discrete states occurs when the velocity of the slide becomes greater than the take-off velocity as shown in Eq. 5.

$$t^* = \min(\tau \geq 0 : \dot{\theta}_{M_2} r_{M_2} > v_{launch}) \tag{5}$$

Where v_{launch} is the take-off velocity. During the climb state, the aircraft and the slide are now detached. To model the aircraft, a 6-DOF standard flat-earth approximation model using Euler angles is utilized [10]. This changes the system states as shown in Eq. 6 to the 12 aircraft states as well as the launch states ($\mathbf{x_{launch}}$).

$$\mathbf{x_{climb}} = \left[\mathbf{p^I}, \dot{\mathbf{p}}^{\mathbf{b}}, \mathbf{\Phi}, \omega^{\mathbf{b}}, \mathbf{x_{launch}} \right] \tag{6}$$

$$\mathbf{p^I} = \left[p_X^I, p_Y^I, p_Z^I \right] \tag{7}$$

$$\dot{\mathbf{p}}^{\mathbf{b}} = \left[\dot{p}_x^b, \dot{p}_y^b, \dot{p}_z^b \right] \tag{8}$$

$$\mathbf{\Phi} = \left[\varphi, \theta, \psi \right] \tag{9}$$

$$\omega^{\mathbf{b}} = \left[w_x^b, w_y^b, w_z^b \right] \tag{10}$$

Where ($\mathbf{p^I}$) is the inertial position of the aircraft as shown in Eq. 7, ($\dot{\mathbf{p}}^{\mathbf{b}}$) is the body-fixed translational velocity of the aircraft as shown in Eq. 8, ($\mathbf{\Phi}$) are the standard Euler angles of the aircraft as shown in Eq. 9, ($\omega^{\mathbf{b}}$) is the body-fixed angular velocity vector as shown in Eq. 10. The control vector is changed to include the control signals of the aircraft as shown in Eq. 11.

$$\mathbf{u}_{climb} = \left[u_a, u_e, u_r, u_f, u_m, u_{M_1}, u_{M_2} \right] \tag{11}$$

Where (u_a, u_e, u_r, u_f) are the aileron, elevator, rudder, and flaps control inputs respectively while (u_m) is the thrust input generated by the aircraft's propellers. The winch motor's dynamics remain the same in the climb phase, while the slide motor's dynamical equations differ due to the detachment from the aircraft which are shown below:

$$\ddot{\theta}_{M_2} = \frac{1}{J_{M_2} + m_s r_{M_2}^2} (-\beta_s r_{M_2}^2 \dot{\theta}_{M_2} - \beta_{M_2} \dot{\theta}_{M_2} + u_{M_2}) \tag{12}$$

The state equations of the inertial position vector $\mathbf{p}^I$ are shown in Eq. 13. These equations form the first set of kinematic differential equations.

$$\dot{\mathbf{p}}^{\mathcal{I}} = \mathbf{L_{VB}} \cdot \dot{\mathbf{p}}^b \tag{13}$$

Where $\mathbf{L_{VB}}$ represents the directional cosine matrix (DCM) which converts a vector from the body-fixed frame to the inertial fixed frame. The time derivatives of the Euler rates form the second set of kinematic equations and are described as shown below:

$$\dot{\phi} = \omega_{X_b} + (\omega_{Y_b} \sin(\phi) + \omega_{Z_b} \cos(\phi)) \tan(\theta) \tag{14}$$

$$\dot{\theta} = \omega_{Y_b} \cos(\phi) - \omega_{Z_b} \sin(\phi) \tag{15}$$

$$\dot{\psi} = \frac{1}{\cos(\theta)} (\omega_{Y_b} \sin(\phi) + \omega_{Z_b} \cos(\phi)) \tag{16}$$

Moving on to the kinetic differential equations, the state equations of the body-fixed velocity vector $\dot{\mathbf{p}}^b$ are as follows:

$$m \cdot \ddot{\mathbf{p}}^b = \mathbf{f}_t^b + \mathbf{f}_g^b + \mathbf{f}_a^b + \mathbf{f}_T^b - m(\omega^b \times \dot{\mathbf{p}}^b) \tag{17}$$

Where $\mathbf{f}_t^b$ is the tether force vector, $\mathbf{f}_g^b$ is the gravitational force vector, $\mathbf{f}_a^b$ is the aerodynamic force vector, and $\mathbf{f}_T^b$ is the thrust force vector. The aforementioned forces are expressed in the body-fixed frame since the differentiation is performed with respect to the body-fixed frame. Regarding the tether force, it consists of the tether aerodynamic force $\mathbf{f}_{t_a}^b$, the tether tension force $\mathbf{f}_{t_\lambda}^b$, and the tether gravitational force $\mathbf{f}_{t_g}^b$.

$$\mathbf{f}_t^b = \mathbf{f}_{t_\lambda}^b + \mathbf{f}_{t_a}^b + \mathbf{f}_{t_g}^b \tag{18}$$

Finally, the last set of state equations describe the evolution of ω^b with time and they form the second set of kinetic differential equations.

$$\mathbf{I}_b \cdot \omega^b = \mathbf{m}_a^b - (\omega^b \times \mathbf{I}_b \cdot \omega^b) \tag{19}$$

Where $\mathbf{I}_b$ is the inertia tensor matrix and $\mathbf{m}_a^b$ is the aerodynamic moment vector. It is important to note that the moment due to the tether is ignored assuming that the attachment point of the tether is very close to the aircraft's center of mass. For more details regarding the model parameters, assumptions, and the external forces and moments, the reader is referred to [8].

C. Controller Design

The control approach proposed in this paper consists of a ground station controller which computes ($\mathbf{u}_{launch}$) and the controller of the aircraft computes $(u_a, u_e, u_r, u_f, u_m)$ based only on local information. This decoupled approach may lead to the system being unaware of possible spikes in the tether tension however, a low tether tension which allows the aircraft

to take-off safely is ensured using the high-level control strategies described below. It is important to note that the high-level control strategies determine the references which are inputted into the system, while the low-level control strategies simply attempt to track these prescribed references.

1) High Level Control Strategy for the Ground Station: The ground station controller consists of the winch motor speed controller, the slide motor position controller and hence in both states, the winch motor is given a speed reference while the slide motor is given a position reference. During the launch phase, a step position reference (θ_{M_2}) is provided to accelerate the slide as quickly as possible over a desired distance (L) which is limited by the rail length of the platform. During this acceleration, the take-off speed (v_{launch}) is reached and the aircraft then separates from the slide. To maintain a low tether tension, the tether must be slack and this is enforced by commanding a velocity reference ($\dot{\theta}_{M_{1_{ref}}}$) shown in Eq. 21. This is the product of the slide motor's velocity and a constant (γ) which is a tunable parameter to ensure a low tether tension in the launch phase. The mathematical expressions of the references are shown in Eq. 20 and Eq. 21.

$$\dot{\theta}_{M_{1_{ref}}} = \gamma \dot{\theta}_{M_{2_{ref}}} \tag{20}$$

$$\theta_{M_{2_{ref}}} = \frac{L}{r_{M_2}} \tag{21}$$

When the required take-off speed of the aircraft is reached, the aircraft is now airborne and the system enters into the climb state where the aircraft is commanded to reach a desired altitude (h_{ref}). Regarding the slide motor, it is simply commanded to maintain its desired position from the launch phase. On the other hand, the winch motor tracks the velocity of the aircraft to maintain the constant slack tether length generated in the launch state. These relations can represented as shown in Eqs.22 and 23 where (r_{M_1}) is the radius of the winch.

$$\theta_{M_{2_{ref}}} = \frac{L}{r_{M_2}} \tag{22}$$

$$\dot{\theta}_{M_{1_{ref}}} = \frac{|\dot{\mathbf{p}}^{\mathbf{b}}|}{r_{M_1}} \tag{23}$$

2) High-Level Control Strategy for the Aircraft: The aircraft's dynamics only appear during the climb state since during the launch state, the slide motor and the aircraft can be considered as one rigid body. To climb to a desired altitude (h_{ref}), the aircraft is provided with reference Euler angles ($\varphi_{ref}, \theta_{ref}, \psi_{ref}$) and a velocity reference on the body-fixed X-axis ($\dot{p}^b_{X_{ref}}$). This is done to maintain a constant climb angle and speed as well as to prevent lateral motion along the inertial Y-axis. Once the aircraft reaches the desired altitude (h_{ref}), it would enter into the transition to crosswind state where the aircraft would steer towards a position suitable to undergo crosswind motion and start the power generation phase. However, the aforementioned flight states are out of the scope of this paper.

3) Low-Level Control of the Ground Station: The slide motor is equipped with a PD controller to achieve its commanded position references in both the launch and climb flight states [11]. The controller was designed neglecting the tether forces considering that the winch's control strategy is designed to keep this force to a minimum essentially decoupling the aircraft and the winch dynamics. The slide motor's control law with a sampling time (T_s) is shown in Eq. 24

$$u_{M_2} = K_{\theta_{M_2}}(\theta_{M_{2_{ref}}}(k) - \theta_{M_2}(k)) - K_{\dot{\theta}_{M_2}}\dot{\theta}_{M_2} \tag{24}$$

The winch motor's controller was designed to track an angular velocity reference. First, the transfer function of the plant was obtained by neglecting the tether tension force in the motor dynamics as shown in Eq. 25.

$$\frac{\dot{\theta}_{M_1}(s)}{u_{M_1}(s)} = \frac{1}{J_{M_1}s + \beta_{M_1}} \tag{25}$$

Where (J_{M_1}) is the moment of inertia of the winch motor and (β_{M_1}) is its viscous friction coefficient. As shown in Eq. 25, the winch dynamics represent a type 0 system hence it would not be able to track a step reference with zero steady-state error. Thus, two integrators were added to increase the order of the system to a type 2 system allowing it to track ramp inputs with zero steady state error which was found to be sufficient for the take-off procedure. The zeros of the system are simply added to pull the integrator poles to the left-hand plane and thus avoid system instability. The transfer function of the controller is shown in Eq. 26.

$$\frac{u_{M_1}(s)}{e(s)} = \frac{41.7(s + Z_1)(s + Z_2)}{s^2} \tag{26}$$

The control parameters of the aforementioned controllers are present in Table I.

TABLE I
CONTROL PARAMETERS FOR THE TAKE-OFF PROCEDURE

Symbol	**Value**	**Unit**
v_{launch}	11	m/s
L	5	m
γ	1.2	–
$K_{\theta_{M_2}}$	14	–
$K_{\dot{\theta}_{M_2}}$	2.5	–
T_s	0.025	s
Z_1	0.4	–
Z_2	0.3	–
h_{ref}	70	m

4) Aircraft controller design using a LQR: To design the LQR controller, the non-linear system was linearized around a steady-level trim point at a speed of around 12 m/s in the

body-fixed X-axis. The tether force and external wind effects are both neglected in the LQR controller and are considered as disturbances from the controller's perspective . To maintain the controllability of the linearized system, the inertial position states $\mathbf{p}^{\mathcal{I}}$ were omitted from the linearization procedure. The state references are as seen in Eq.33 taking into consideration the omission of the position states. The weighting matrices were tuned such that the input constraints are satisfied under the given operating conditions while maintaining acceptable tracking performance. The weighting matrices for the states and the controls are as follows:

$$diag\{\mathbf{Q_{LQR}}\} = \Big[1e2, 0, 0, 1e2, 5e4, 1e2, 1e3, 1e2, 1e3\Big] \quad (27)$$

$$diag\{\mathbf{R_{LQR}}\} = \Big[1e5, 7.5e5, 1e5, 1e5, 1e-1\Big] \quad (28)$$

5) Aircraft controller design using a NMPC: Due to the highly non-linear dynamics of AWE systems, their uncertain operating environments, and hard input constraints, an NMPC controller is proposed as the low-level controller for the aircraft. The NMPC is introduced in the climb state, when the aircraft is separated from the slide and made to track the references $(\phi_{ref}, \theta_{ref}, \psi_{ref}, \dot{p}^b_{X_{ref}})$ capturing the high-level control strategy. The hyperparameters were chosen such that the Optimal Control Problem (OCP) benefits from a high control frequency (f_{NMPC}) with a sufficiently large prediction horizon (N_{NMPC}). A large horizon is utilized to ensure that spikes in the tether tension are anticipated early enough for corrective action however, it is not excessively long to allow for real-time computational time. A high control frequency on the other hand, maintains the reactivity of the system against model uncertainties and disturbances. The set of hyperparameters that were found to perform well while being computationally feasible are shown in Eq. 29.

$$N_{NMPC} = 20, \; f_{NMPC} = 40Hz \quad (29)$$

A non-linear quadratic least squares cost function (J_{NMPC}) is chosen for the NMPC controller as shown in Eq. 30.

$$\begin{aligned} J_{NMPC} = {} & (\mathbf{x_N} - \mathbf{x_{N_{ref}}})^T \, \mathbf{S_{MPC}} \, (\mathbf{x_N} - \mathbf{x_{N_{ref}}}) \\ & + \sum_{k=0}^{N_{NMPC}-1} ((\mathbf{x_k} - \mathbf{x_{k_{ref}}})^T \, \mathbf{Q_{NMPC}} \, (\mathbf{x_k} - \mathbf{x_{k_{ref}}}) \\ & \quad + (\mathbf{u_k} - \mathbf{u_{k_{ref}}})^T \, \mathbf{R_{NMPC}} \, (\mathbf{u_k} - \mathbf{u_{k_{ref}}})) \end{aligned} \quad (30)$$

Where $(\mathbf{x_k})$ and $(\mathbf{u_k})$ are the state and control vectors in the Lagrange term of the cost function, $(\mathbf{x_{k_{ref}}})$ and $(\mathbf{u_{k_{ref}}})$ are the reference state and control vectors in the Lagrange term of the cost function, $(\mathbf{x_N})$ and $(\mathbf{x_{N_{ref}}})$ are the terminal state vector and its reference in the Mayer term of the cost function.

The reference state and control vectors utilized to achieve the aforementioned goals of the climb phase are shown in Eq. 31 and Eq. 32.

$$\mathbf{x_{k_{ref}}} = \mathbf{x_{N_{ref}}} = [\mathbf{p^{\mathcal{I}}_{ref}} \; \dot{\mathbf{p}}^{\mathbf{b}}_{\mathbf{ref}} \; \mathbf{\Phi_{ref}} \; \omega^{\mathbf{b}}_{\mathbf{ref}}]^T \quad (31)$$

$$\mathbf{u_{k_{ref}}} = [u_{a_{ref}} \; u_{e_{ref}} \; u_{r_{ref}} \; u_{f_{ref}} \; u_{m_{ref}}]^T \quad (32)$$

Where:

$$\mathbf{p^{\mathcal{I}}_{ref}} = [0,0,0]^T \quad \dot{\mathbf{p}}^{\mathbf{b}}_{\mathbf{ref}} = [11,0,0]^T \quad \mathbf{\Phi_{ref}} = [0°, 40°, 0°]^T$$

$$\mathbf{w^b_{ref}} = [0,0,0]^T \qquad \mathbf{u_{k_{ref}}} = [0,0,0,0,0]^T \quad (33)$$

The weights were chosen to result in a dimensionless cost function, leading to consistent converge of the NMPC. The weighting matrices present in Eq. 30 are shown in Eq. 34, 35 and 36.

$$diag\{\mathbf{Q_{NMPC}}\} = \Big[0, 0, 0, 1e1, 0, 0, 1e3, 1e4, 1e2, 1e2, 1e2, 1e2\Big] \quad (34)$$

$$diag\{\mathbf{R_{NMPC}}\} = \Big[1e1, 1e5, 1e1, 1e4, 1e1\Big] \quad (35)$$

$$diag\{\mathbf{S_{NMPC}}\} = diag\{\mathbf{Q_{NMPC}}\} \quad (36)$$

The units of each state variable are taken into consideration when defining the weights such as to yield a dimensionless cost. Note that states whose weights are equal to zero are not penalized in the cost function. One of the many advantages of using NMPC is that state and input constraints are considered directly in the OCP formulation. In the context of this paper, only control input constraints will be considered. The aileron u_a, elevator u_e, rudder u_r, and flaps u_f are restricted between $-0.35 \; rad$ and $0.35 \; rad$. Additionally, the thrust input u_m is constrained between $0 \; N$ and $20 \; N$. The solver is set up with the hyperparameters shown in Table II which yielded good and consistent convergence.

TABLE II
HYPERPARAMETERS OF NMPC CONTROLLER OF CLIMB PHASE

Parameter Name	**Symbol**	**Value**
Prediction Horizon	N_{NMPC}	20
Control Frequency	f_{NMPC}	$40 \; Hz$
SQP Newton's Step Size	$\alpha_{SQP_{NMPC}}$	1.0
Simulation Method	-	explicit-runge kutta
Simulation Number of Stages	$n_{stages_{NMPC}}$	4
Simulation Number of Steps	$n_{steps_{NMPC}}$	1
Regularization Method of QP algorithm	-	convexify

D. NMPC solver

Within this work, acados [12] is used as the NMPC solver which is an open-source software package providing fast and embedded solvers for non-linear OCPs. This solver is optimized for small to medium sized systems consisting of up to 20 states and performs optimally with quadratic cost functions and smaller prediction horizons, which is due to its optimized

sensitivity analysis and structure exploiting SQP. Considering that our system fits the aforementioned description and considering acados's embedded code generation capabilities, it was the chosen solver for the NMPC controller presented in this paper.

III. Results

The model and control system were implemented in Matlab/Simulink [13] using enabled subsystems that represented system dynamics during both the launch and climb phases. In the simulations, once the aircraft reached take-off speed, a positive control signal triggered the climb phase. The NMPC controller was integrated via an S-function generated using acados's [12] Matlab/Simulink interface. Simulations ran for about ten seconds to allow both phases to execute. It was assumed that after this period, the system entered the transition to crosswind flight, which is beyond this paper's scope. The NMPC averaged a 13.5 ms execution time, while the LQR ran in about 10 μs. Both were faster than the system's sampling time, supporting real-time implementation. Wind disturbances were not modeled, limiting robustness evaluation—particularly for the LQR, which was trimmed for a specific wind speed.

In the ground station simulations, only minor differences were observed between the results using the LQR and NMPC controllers, primarily due to the similar magnitudes of the tether forces. This similarity is further reinforced by the decoupling of the aircraft and ground station control, as both the slide and winch motors are regulated by PID controllers. Their only interaction with the aircraft is via the tether force, which acts as a disturbance from the PID's perspective. Figure 3 shows the slide motor's angular position, illustrating its ability to track and hold its reference despite tether disturbances. During the initial acceleration phase, the aircraft remains attached to the slide, but after approximately 0.5 s, it detaches, and the slide maintains its position.

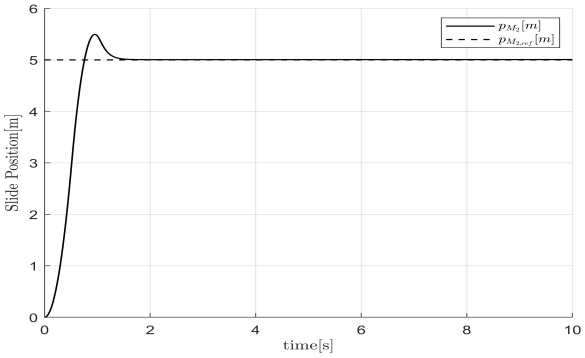

Fig. 3. Slide motor angular position response during linear take-off procedure for the LQR and NMPC controllers

Regarding the winch motor, Figure 4 shows that it tracks its velocity reference with minimal steady-state error. This error arises from the tether force, which was neglected during control design. The sudden drop in reference velocity corresponds to the transition from the launch to climb phase, where the winch's reference changes due to differing high-level control strategies, as described in Eqs. 20 and 23. The winch behavior under the NMPC controller is nearly identical, achieving similarly accurate tracking; therefore, its figure was omitted to avoid redundancy.

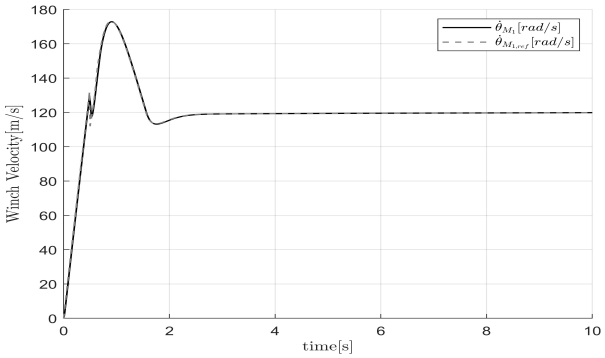

Fig. 4. Winch motor angular velocity response during linear take-off procedure for the LQR controller

The aircraft trajectories during the take-off phase are shown in Figure 5. As seen in the graph, the aircraft moves only in the X-Z plane, so the inertial Y-axis position is omitted. During the first ten seconds, the NMPC controller drives the aircraft to a higher altitude, about 70 meters, compared to 60 meters with the LQR. This highlights NMPC's superiority in altitude gain, which is crucial for quickly reaching the target altitude and minimizing energy losses that reduce the energy conversion efficiency of AWE systems [6]. The launch phase comprises the first 0.5 seconds, during which the aircraft's velocity lies solely along its body-fixed X-axis and matches the slide motor's velocity, as both behave as a rigid body in this phase.

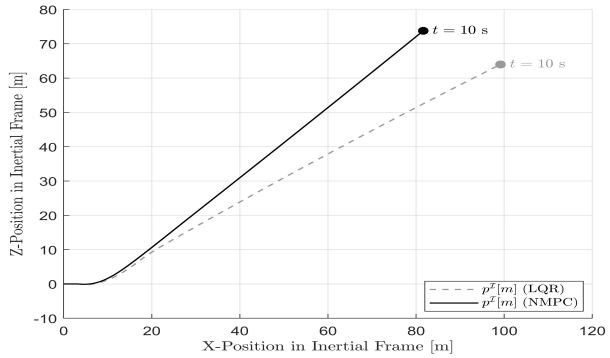

Fig. 5. Position response for the rigid wing AWE system in the Inertial frame during linear take-off procedure with the LQR and NMPC controllers

Moving on to the body-fixed velocities, it can be seen from Figure 6 that the aircraft with a NMPC controller is able

to track its reference velocity in the body-fixed X-axis with minimal steady state error within the ten second time frame. However, it is apparent that the velocity slightly decreases with time and this is due to the increasing tether line length leading to a large tether drag force which eventually cannot be overcome by the thrust force of the aircraft. This is why the system must enter into the transition to crosswind phase as soon as possible. The initial overshoot is quite large which is due to the fact that a maximum thrust is initially applied to pitch the aircraft upwards and as the aircraft reaches its required pitch angle, the velocity converges to its reference. The body-fixed velocities with the LQR controller can be observed in Figure 6. Initially, there is a large overshoot comparable to that of the NMPC controller which is also due to the large thrust applied initially. However, the steady state error is quite large where the velocity in the body fixed X-axis stabilizes at around $11.6\ m/s$, which indicates the superiority of the NMPC in handling the tether forces and inherent non-linearities of the system.

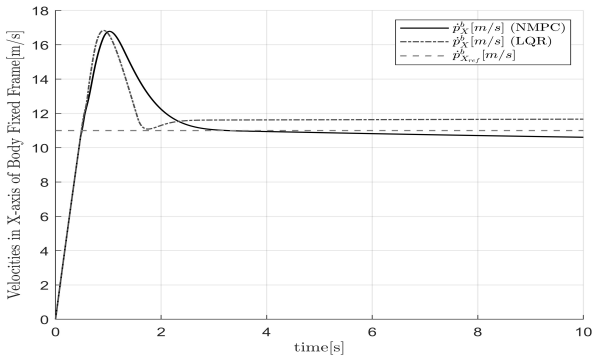

Fig. 6. Velocity response for the rigid wing AWE system in the Body fixed frame during linear take-off procedure with the LQR and NMPC controllers

The pitch angle trajectory for the NMPC and LQR controllers can be observed in Figure 7. The NMPC successfully tracks the reference pitch angle of $40°$ and maintains it with a minor steady-state error to gain altitude as quickly as possible. On the other hand, the LQR controller is unable to track the pitch angle to a large extent and never reaches steady state. This implies that the system is driven away from its operating point making the linearized model ineffective. The presence of the tether force; more specifically the increasing tether drag force; can explain these results since it was neglected in the design of the LQR, however, this force increases the non-linearities of the system making the controller unable to track its required pitch angle. Attempts to mitigate this behavior were unsuccessful as the typically control constraints are violated. For larger desired altitudes, it is apparent that the LQR controller may eventually cause a drop in altitude making it especially ineffective if wind speeds are low and the aircraft must be driven to higher altitudes. During the launch phase, the pitch angle was assumed to be zero assuming the aircraft's nose is parallel to the inertial X-axis.

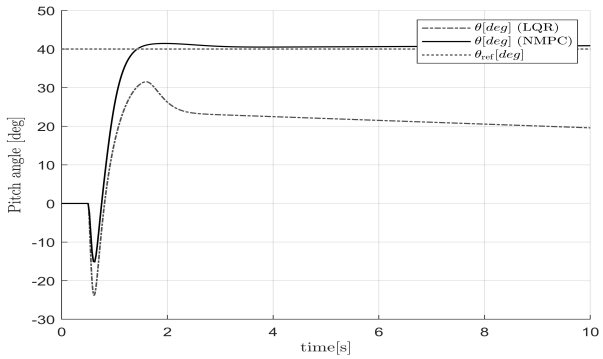

Fig. 7. Pitch (θ) response for the rigid wing AWE system during linear take-off procedure for the LQR and NMPC controllers

Figure 8 show the magnitude of the tether force with the NMPC and LQR controllers. The tether force in both cases is maintained below a value of 10 N which indicates that the winch's high-level control strategy was successful in maintaining a low tether tension. This is required to prevent any unwanted spikes in the tether tension which could possibly halt the take-off procedure. Furthermore, during the launch phase, the tether force is zero since a slack length is maintained and the tether drag and weight forces are assumed to be negligible considering that the aircraft is not yet airborne. There is no significant difference between the LQR and NMPC controllers in terms of the tether force since the high-level control strategy of the winch tracks the velocity of the aircraft irrespective of the value. However, it is apparent that the tether force in the LQR controlled aircraft is increasing at a larger rate than that of the MPC. This can be attributed to the larger velocities associated with the LQR controller which lead to larger tether drag forces. The steady increase of the tether force with time is due to the increase in the tether length as the winch reels out which causes an increase in tether drag, however, after the first ten seconds it is assumed that the aircraft would enter the transition phase and hence the winch would start reeling in leading to lower tether drag forces.

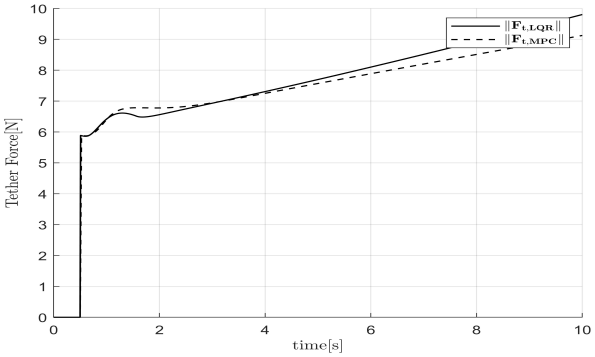

Fig. 8. Tether force magnitude acting on the rigid wing AWE system during linear take-off procedure with the NMPC and LQR controllers

To assess power efficiency, the power required for take-off was computed for the winch motor, slide motor, and aircraft, as shown in Figures 9 and 10. The peak total power dissipation reached approximately $6.2\ kW$ for LQR and $6.0\ kW$ for NMPC as shown in Figures 9 (d) and 10 (d) . At steady state, power losses rose to around $0.77\ kW$ and $0.56\ kW$, respectively, mainly due to higher power dissipation in the aircraft and winch motor under LQR. Although both controllers use the same PID for the winch (Figures 9 (b) and 10 (b)), LQR's steady-state velocity error leads to higher speed references and thus higher losses. Propulsion power (Figures 9 (c) and 10 (c)) also shows a smaller loss difference of $20\ W$, attributed to reduced tether forces with NMPC. Slide motor power is nearly identical due to the use of the same PID controller and similar values for the tether force. Over $10\ s$, NMPC achieved $70\ m$ altitude vs. $60\ m$ for LQR, confirming NMPC's superior energy efficiency.

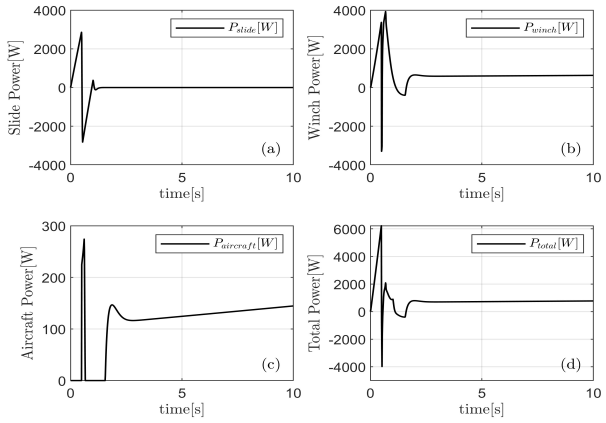

Fig. 9. Power dissipated in the slide motor, winch motor, aircraft propulsion, and the total power dissipated in the system when employing the LQR controller in the climb phase

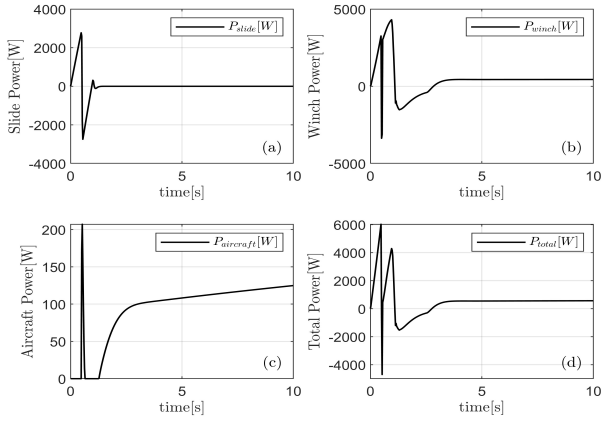

Fig. 10. Power dissipated in the slide motor, winch motor, aircraft propulsion, and the total power dissipated in the system when employing the NMPC controller in the climb phase

IV. Conclusion

This paper proposed an NMPC controller to implement a linear take-off procedure for a hybrid rigid wing AWE system. PID controllers were designed for the winch and slide motors during both the launch and climb states, while the NMPC and LQR controllers were implemented in the climb state to control the highly non-linear dynamics of the aircraft under hard input constraints. Simulations results show that the NMPC is able to track the state references with minimal steady state error while satisfying the control constraints even in the presence of continuously increasing tether forces. The LQR controller however, exhibited larger steady state error, especially in the pitch angle and body-fixed velocities, as compared to the NMPC and its tracking performance worsened at larger altitudes where larger tether forces appear. Finally, in terms of energy efficiency, the NMPC controller exhibited its superiority where it is able to drive the system to larger altitudes with lower power losses making it essential for highly efficient AWE systems.

References

[1] C. Vermillion, M. Cobb, L. Fagiano, R. Leuthold, M. Diehl, R. Smith, T. Wood, S. Rapp, R. Schmehl, D. Olinger, and M. Demetriou, "Electricity in the air: Insights from two decades of advanced control research and experimental flight testing of airborne wind energy systems," *Annual Reviews in Control*, 04 2021.

[2] M. L. Loyd, "Crosswind kite power (for large-scale wind power production)," *Journal of Energy*, vol. 4, no. 3, pp. 106–111, 1980.

[3] P. Bechtle, M. Schelbergen, R. Schmehl, U. Zillmann, and S. Watson, "Airborne wind energy resource analysis," *Renewable Energy*, vol. 141, 04 2019.

[4] A. F. Pereira and J. M. Sousa, "A review on crosswind airborne wind energy systems: key factors for a design choice," *Energies*, vol. 16, no. 1, p. 351, 2022.

[5] L. Fagiano, E. Nguyen-Van, F. Rager, S. Schnez, and C. Ohler, "Autonomous takeoff and flight of a tethered aircraft for airborne wind energy," *IEEE transactions on control systems technology*, vol. 26, no. 1, pp. 151–166, 2017.

[6] L. Fagiano and S. Schnez, "On the take-off of airborne wind energy systems based on rigid wings," *Renewable Energy*, vol. 107, pp. 473–488, 2017.

[7] L. Fagiano, E. Nguyen Van, F. Rager, S. Schnez, and C. Ohler, "Automatic take-off of a tethered aircraft for airborne wind energy: Control design and experimental results," *IFAC-PapersOnLine*, vol. 50, pp. 11932–11937, 07 2017.

[8] E. Nguyen Van, L. Fagiano, and S. Schnez, "On the autonomous take-off and landing of tethered wings for airborne wind energy," in *2016 American Control Conference (ACC)*, pp. 4077–4082, 2016.

[9] M. Zanon, S. Gros, and M. Diehl, "Rotational start-up of tethered airplanes based on nonlinear mpc and mhe," pp. 1023–1028, 07 2013.

[10] E. N. Van, L. Fagiano, and S. Schnez, "Autonomous take-off and landing of a tethered aircraft: a simulation study," *arXiv preprint arXiv:1510.01088*, 2015.

[11] L. Fagiano, E. Nguyen-Van, F. Rager, S. Schnez, and C. Ohler, "A small-scale prototype to study the takeoff of tethered rigid aircrafts for airborne wind energy," *IEEE/ASME Transactions on Mechatronics*, vol. 22, no. 4, pp. 1869–1880, 2017.

[12] R. Verschueren, G. Frison, D. Kouzoupis, J. Frey, N. v. Duijkeren, A. Zanelli, B. Novoselnik, T. Albin, R. Quirynen, and M. Diehl, "acados—a modular open-source framework for fast embedded optimal control," *Mathematical Programming Computation*, vol. 14, no. 1, pp. 147–183, 2022.

[13] T. M. Inc., "Matlab version: 24.2.0.2773142 (r2024b)," 2024.